Nanoscale

Skyrmion lattice formation and destruction mechanisms probed with TR SANS

Journal:	*Nanoscale*
Manuscript ID	NR-ART-02-2024-000858.R1
Article Type:	Paper
Date Submitted by the Author:	17-Apr-2024

Complete List of Authors:	Liyanage, WLNC; The University of Tennessee Knoxville College of Arts and Sciences, Physics Tang, Nan; University of Tennessee Knoxville College of Engineering, Materials Science and Engineering Dally, Rebecca; NIST Center for Neutron Research Quigley, Lizabeth; University of Tennessee Knoxville College of Engineering, Materials Science and Engineering Buchanan, Charlotte; The University of Tennessee Knoxville, Materials Science and Engineering Shu, Guo-Jiun; National Taipei University of Technology, Materials and Mineral Resources Engineering Butch, Nicholas; NIST Center for Neutron Research; University of Maryland Krycka, Kathryn; NIST Center for Neutron Research Bleuel, Markus; NIST Center for Neutron Research; Louisiana State University Debeer-Schmitt, Lisa; Oak Ridge National Laboratory, Neutron Scattering Sciences Division Borchers, Julie; National Institute of Standards and Technology, NIST Center for Neutron Research Gilbert, Dustin; University of Tennessee Knoxville College of Engineering, Material Science and Engineering and Physics & Astronomy

Skyrmion lattice formation and destruction mechanisms probed with TR-SANS

WLNC Liyanage,[1] Nan Tang,[2] Rebecca L. Dally,[3] Lizabeth J. Quigley,[2] C. Charlotte Buchanan,[2] Guo-Jiun Shu,[4,5] Nicholas P. Butch,[3,6] Kathryn Krycka,[3] Markus Bleuel,[3,7] Julie A. Borchers,[3] Lisa Debeer-Schmitt,[8] Dustin A. Gilbert[1,2]

[1] Department of Physics and Astronomy, University of Tennessee, Knoxville, TN 37996, USA
[2] Materials Science Department, University of Tennessee, Knoxville, TN 37996, USA
[3] NIST Center for Neutron Research, National Institute of Standards and Technology, Gaithersburg, MD 20899, USA
[4] Center for Condensed Matter Sciences, National Taiwan University, Taipei 10617, Taiwan
[5] Department of Materials and Mineral Resources Engineering, Institute of Mineral Resources Engineering, National Taipei University of Technology, Taipei 10608, Taiwan
[6] Center for Nanophysics and Advanced Materials, Department of Physics, University of Maryland, College Park, MD 20742, USA
[7] Department of Materials Science and Engineering University of Maryland College Park, College Park, MD 20742, USA
[8] High Flux Isotope Reactor, Oak Ridge National Laboratory, Oak Ridge, TN 37830, USA

ABSTRACT

Magnetic skyrmions are topologically protected, nanoscale whirls of the spin configuration that tend to form hexagonally ordered arrays. As a topologically non-trivial structure, the nucleation and annihilation of the skyrmion, as well as the interaction between skyrmions, varies from conventional magnetic systems. Recent works have suggested that the ordering kinetics in these materials occur over millisecond or longer timescales, which is unusually slow for magnetic dynamics. The current work investigates the skyrmion ordering kinetics, particularly during lattice formation and destruction, using time-resolved small angle neutron scattering (TR-SANS). Evaluating the time-resolved structure and intensity of the neutron diffraction pattern reveals the evolving real-space structure of the skyrmion lattice and the timeframe of the formation. Measurements were performed on three prototypical B20 skyrmion materials: MnSi, (Fe,Co)Si, and Cu_2OSeO_3. To probe lattice formation and destruction kinetics, the system was prepared in the stable skyrmion state, and then a square-wave magnetic field modulation was applied. The measurements show that the skyrmions form ordered domains very quickly, with a significant distribution in lattice parameters, which then converge to the final structure; the results confirm the slow kinetics, with formation times between 10 ms and 99 ms. Comparisons are made between the measured formation times and the fundamental material properties, suggesting the ordering temperature, saturation magnetization and magnetocrystalline anisotropy may be driving the timeframes. Micromagnetic simulations were also performed and support a scaling of the kinetics with sample volume, an artifact which is caused by the reconciling of misaligned domains.

INTRODUCTION

Chiral spin textures have been the focus of intense research in condensed matter physics due to their unconventional structure, their resulting field response and their magnetic dynamics.[1-3] Among these magnetic structures, skyrmions have been a recent focus due to their non-trivial topology and associated quasiparticle behaviors.[4-6] The structure of the skyrmion can be generally described as a continuous coplanar wrapping of the magnetic moments, with a core and fencing perimeter that are oriented in opposite out-of-plane directions. This very specific configuration is the origin of the topological protection and is what makes the nucleation and annihilation of skyrmions a non-trivial event, resulting in a change in the total topology of the system.[7-9] In many skyrmion materials these structures order into hexagonal arrays, allowing them to be readily detected with small angle neutron scattering.[10-14] In materials with a Dzyaloshinskii-Moriya interaction (DMI), the direction of the coplanar wrapping is the same for each skyrmion, allowing a hexagonally ordered skyrmion lattice to alternatively be described as a 3-q helical structure, e.g. an extended magnetic configuration consisting of three coherent helices located at 60° relative in-plane angles.

The ordering of the skyrmion lattice is primarily determined by the balance between the direct exchange interaction[15] and the antisymmetric DMI; the magnetostatic interactions,[16] magnetocrystalline, Zeeman,[17] and thermal energies also contribute, but are generally considered much weaker than the exchange terms. These energy terms together result in the skyrmions achieving stability in a tiny pocket in the magnetic field – temperature (H-T) parameter space, typically near the Curie temperature (T_c),[17] indicating the importance of thermal fluctuations.

Recent works have suggested the timescales of skyrmion kinetics are fundamentally different, and in-particular much slower, compared to typical magnetic dynamics, which occur on the nanosecond timeframe. [1, 17, 18] One study by Bannenberg *et al*., showed that moving the lattice, e.g. reorientation, can occur over hundreds of seconds.[17] In another study, Wilson *et al.*, used electric fields to nucleate a magnetic skyrmion lattice in zinc substituted Cu_2OSeO_3, finding that the lattice forms in 10-10,000 seconds depending on the field and temperature, and the energy barrier of formation is in the millielectronvolt range.[1] In a third work, Nakajima et al. performed time-resolved SANS measurements during cooling and warming cycles in an MnSi crystal and reported formation times on the order of 100 ms.[19] The discrepancy between the nucleation timescale and lattice ordering dynamics, approximately ten orders of magnitude is a surprise and bring into question the mechanics underlying the lattice ordering. Key among these considerations when treating the system as a 3-q helix is that ordering is expected to occur by simple propagation of the helix. These experimental works hint at slow lattice dynamics, with one describing collective motion, and the other using an electric field to distort the energy landscape; most skyrmion works manipulate the skyrmion lattice with temperature or magnetic field, raising the question if slow kinetics also exist for these controls.

In this study we use time resolved small angle neutron scattering experiments (TR-SANE)[20, 21] in three different B20 bulk materials (MnSi, $Fe_xCo_{1-x}Si$, Cu_2OSeO_3) to investigate the nucleation and annihilation kinetics of the skyrmion lattice. The experiment was performed by preparing the system near the boundary of the skyrmion stability window and then stepping the magnetic field, moving the system into and out-of the skyrmion stabilizing pocket, resulting in lattice formation and destruction. The diffraction pattern as a function of time is captured during the field stepping. Formation dynamics were measured at both the high-field and low-field boundaries of the stability envelopes for each material, as well as using different field steps, demonstrating the role of the magnetic field. The present study shows that the nucleation and annihilation events occur over millisecond time scales and are different among the

investigated materials. Insights into the formation kinetics are extracted by evaluating changes in the diffraction pattern versus time. Discussions are provided which compare the fundamental magnetic energies in the three materials and correlations with the formation timeframes.

METHODS

Bulk single crystal MnSi, Cu_2OSeO_4 (COSO), and $Fe_{0.85}Co_{0.15}Si$ (FCS) samples were used for the experiments, and were prepared as described previously [11, 20, 22].

Neutron scattering experiments were performed using the NG7 beamline at the NIST Center for Neutron Research [23]. Each sample was cooled in a closed cycle refrigerator to the measurement temperature and placed within an electromagnet, with the field aligned along the neutron beam direction; this field will be called the quasistatic field. An unpolarized neutron beam with a wavelength (λ) of 6 Å ($\Delta\lambda/\lambda$ = 13%) was used. A second coil is placed around the sample, with the coil axis also parallel to the neutron beam, which is used to apply a bipolar step field; this will be called the dynamic field. Samples were mounted in a boronated aluminum aperture, with Cd shielding to reduce background scattering. 2D SANS images in the provided figures are representative of the quasi-static condition, taken between the field steps.

Once the sample is cooled to the measurement temperature, the quasistatic field is increased to saturation and then decreased in small steps until a hexagonal diffraction pattern appears in the SANS detector, identifying the boundary of the skyrmion stability pocket. Next, the secondary coil for the dynamic field is energized using a bipolar square wave current with a frequency of 0.1 Hz, switching between positive and negative polarity, such that the magnetic field is outside\inside the stabilizing pocket on the phase diagram to annihilate\nucleate the skyrmion lattice, as identified by arrows labeled 1 and 2 in Fig. 1 (a). Each neutron count was recorded and included a timestamp with approximately nanosecond resolution. For each measurement, SANS data were collected continuously for 2 hours. The data were then combined into 10 ms bins, and then further discretized into 10 second frames that represent the periodic dynamic field. The bins were averaged over all of the frames, resulting in a 10 second duration dataset consisting of (q_x, q_y, I, t), where I is the intensity at the wavevector coordinates (q_x, q_y) at time t, with 10 ms resolution. With this data the time-resolved evolution of the diffraction pattern can be viewed. To quantitatively evaluate the evolution, the patterns were each circularly averaged around the 2D detector, generating an I versus q plot, or averaged over a range of wavevector radii that included the diffraction pattern from the skyrmions, generating an I versus ϕ plot. Integrating the intensity of the entire 2D diffraction pattern provides the total intensity of the diffraction pattern at each time step, generating an I versus t plot. IgorPro [24] and Grasp[25] softwares were used to reduce the data and subtract the background. Creation\destruction time constants are calculated by fitting sigmoidal or exponential functions for the I versus t graphs, as discussed below. To evaluate the position and width of the diffraction peaks at each timestep the data were fit using one Gaussian for the I versus q data, or six coupled Gaussians constrained to be separated by 60° for the I versus ϕ data. The 13% wavelength distribution results in a 4 ms smearing of the data (between the fastest 5.22 Å and slowest 6.78 Å neutrons). Similar measurements are performed at the lower field boundary, which is identified by increasing the quasistatic field from H=0 until the hexagonal diffraction pattern appears.

RESULTS

MnSi

As the first sample, MnSi is used.[15] In the MnSi H-T phase diagram, skyrmions exist within a small pocket of temperatures between the Curie temperature (T_c), 29.5 K, and 27.5 K, and a pocket of magnetic fields between 100 mT to 250 mT applied along the [111] axis. The MnSi sample was zero field cooled (ZFC) to the test temperature (28.8 K). The quasistatic magnetic field was next aligned with the neutron beam and [110] axis of the MnSi crystal, and then a 500 mT saturating field was applied. The field was incrementally decreased until the hexagonal diffraction pattern was observed in the SANS detector, at 250 mT, corresponding to the high field boundary of the skyrmion pocket. A hexagonal scattering pattern was observed at q = (3.8± 0.1) $\times 10^{-2}$ Å^{-1} (Fig. 1 (b)), corresponding to the real space skyrmion lattice spacing of 165 ± 4 Å. Some peaks appeared brighter due to a slight misalignment between the magnetic field and the neutron beam.

The dynamic field was then applied with a magnitude of ±13 mT and the time-resolved SANS pattern was captured. These fields move the state across the high field boundary of the skyrmion pocket and into the conical phase. The field is rapidly increased from 250 mT to 263 mT and the hexagonal pattern disappears from the SANS detector (Fig. 1 (c)), confirming that the sample is out of the skyrmion stability pocket. Next, five seconds later, the magnetic field is decreased to 237 mT and the hexagonal pattern returns, indicating the system is back within the skyrmion stability pocket. Similar measurements were performed using a dynamic field of ±38 mT, resulting in similar observations. It is notable that the scattering intensity at 212 mT was larger than at 237 mT, despite both being within the skyrmion stability pocket. This may indicate that domains exist within the sample that have not transformed to the skyrmion state at 237 mT, or that the shape of the skyrmions, which contributes the scattering form factor, is different. This decrease in intensity was observed previously in dipole stabilized skyrmion lattices,[14, 26] however is unexpected here since the exchange dominated skyrmions are much more rigidly defined.

Following the sequence discussed in the Methods section, the time resolved diffraction pattern is determined and the intensity vs. time graphs are compiled, Fig. 1(d) and (e). During the transition from the conical phase to skyrmion phase no scattering was observed; the scattering intensity continuously and simply transforms from nothing to the hexagonal structure. This indicates that either we do not have the time resolution to capture a disordered phase, or more likely, the skyrmion lattice nucleates and grows into domains rather than large areas of disordered structures, although there are a range of features that may exist in the dynamic state.[27] A stepwise exponential function was used to fit the change in diffraction intensity and determine the time constants for the creation and destruction of the skyrmion lattice. For the creation of the skyrmion lattice (red curve in Fig. 1(d)) the following functions were used:

$$\begin{cases} d & t < t_0 \\ c\left(1 - e^{-\frac{(t-t_0)}{\tau}}\right) + d & t \geq t_0 \end{cases}$$

Also, for the destruction of the skyrmion lattice, the following functions were used (red curve in Fig. 1 (e)).

$$\begin{cases} c + d & t < t_0 \\ c\left(e^{-\frac{(t-t_0)}{\tau}}\right) + d & t \geq t_0 \end{cases}$$

In the above functions c, t_0, τ, d represent the scattering intensity at 3.5 Å^{-1} < q < 4.1 Å^{-1}, coinciding with diffraction from the skyrmion lattice, the time in the measurement frame of reference, the time constant, and a vertical offset of the background intensity, respectively. The critical parameter we consider here is the time constant (τ).

The converged value for τ is 42.71 ± 0.03 ms for the formation of the skyrmion lattice at the top boundary with the large field step (288 mT to 212 mT). For the smaller field step (263 mT to 237 mT), τ increased to 47.8 ± 0.05 ms. These values show that increasing the field step size causes the time constant for skyrmion lattice formation at the upper boundary to decrease. The converged values for skyrmion lattice destruction are much faster, with τ= 10.36 ± 0.03 ms and 18.0 ± 0.01 ms for the large (±38 mT) and small (±13 mT) field steps, respectively. This result again shows that the larger the field step, the faster the transformation.

At the lower boundary of the skyrmion stability pocket (160 mT) the formation time constant was determined to be 21.4 ± 0.1 ms for the large field step of (122 mT to 198 mT, ±38 mT), notably faster than the upper boundary, while the destruction time constant is 18.97 ± 0.02 ms for (198 mT to 122 mT).

For the small field step (±13 mT) at the lower boundary (148 mT to 172 mT) the skyrmion lattice does not fully disappear, having a residual intensity of ≈10%, but the destruction and formation timeframes can still be tabulated. The destruction time was found to be the largest so-far (50.9 ± 0.03 ms). Though one might then expect that the formation time was much shorter, growing from an already-nucleated landscape, the formation time was also very long (44.32 ± 0.05 ms).

$Fe_xCo_{1-x}Si$

The formation and destruction times of the skyrmion lattice in $Fe_xCo_{1-x}Si$ (x= 0.85, hereafter abbreviated as FCS) were also measured. This material provides a complementary skyrmion lattice with a different skyrmion periodicity and stability window (temperature and field ranges), as well as contrasting underlying exchange-constants. As another prototypical skyrmion-harboring B20 material, FCS shows a skyrmion lattice near the Curie temperature of ≈22 K, which is much colder than MnSi.[28-30] The sample was ZFC to 20.5 K. A magnetic field was next applied parallel to the neutron beam and the crystal [001] direction.[31, 32] Using the procedure described above, the boundaries of the skyrmion stability envelope were identified with SANS and then the nucleation and annihilation events were investigated using dynamic field steps of (±10 mT and ±5 mT); smaller fields were chosen to reflect the much smaller stability window.

The high-field and low-field boundaries of the skyrmion pocket were found to be 55 mT and 20 mT, respectively. Using a dynamic field of ±10 mT at the upper field boundary, the scattering pattern inside the skyrmion stability window at $\mu_0 H$=45 mT, shown in Fig. 2(a), does not reproduce the hexagonal pattern generated by the adiabatic sequence. Rather, the scattering pattern appears as an inhomogeneous ring with a radius q = (1.5 ± 0.1) ×10^{-2} Å^{-1}, corresponding to a real space skyrmion lattice spacing of 419 ± 28 Å. The appearance of a ring inside of the skyrmion stability envelope suggests either the system instead forms labyrinth domains or that the skyrmions form with short-range order but no long-range orientation.[33] This pattern was observed previously in this sample, and by slowly turning the sample in a static field, resolves to a hexagonal diffraction pattern, suggesting the system consists of misoriented

skyrmion domains. The long-range correlation of skyrmion domains is determined by the magnetocrystalline coupling and is optimized when measuring in a plane with a single easy-axis vector in the plane orthogonal to the field. [33] The different microscopic orderings between the dynamic and adiabatic measurements may be the result of the large number of simultaneously nucleated domains in the former, while the latter generates fewer domains that propagate and grow. Alternatively, the dynamic measurements may leave residual nucleation sites[34] that define a local orientation.

Following the measurement sequence, the field was stepped to 65 mT, at which point the diffraction pattern disappears (Fig. 2(b)). The intensity of the diffraction pattern was once-more extracted from each 10 ms frame and the creation and destruction time constants calculated. Time constants for the formation and destruction of the skyrmion lattice at the upper field boundary were determined to be 70.28 ± 0.06 ms and 35.49 ± 0.03 ms for field steps of ±10 mT, and 72.1 ± 0.06 ms and 58.28 ± 0.05 ms for smaller field steps of ±5 mT, respectively. This again is consistent with smaller steps resulting in longer formation and destruction timeframes. Also notable, these parameters are slower than the MnSi upper boundary.

Data were also collected at the lower boundary of the skyrmion stability envelope, centered at 20 mT with the field steps of ±5 mT and ±10 mT. At both 25 mT and 30 mT the system is inside the skyrmion stability envelope and the scattering pattern shows a hexagon imposed over a uniform ring (Fig 2(c)). As the measurement field is reduced outside of the skyrmion stability envelope, the scattering pattern mostly disappears, however two weak diffraction peaks are observed along the Q_y direction (Fig. 2(d)). These two peaks confirm the destruction of the skyrmion lattice and indicate a helical structure along the Y-direction. Time constants for the formation and destruction of the skyrmion lattice at the lower field boundary were measured to be 71.19 ± 0.05 ms and 20.22 ± 0.03 ms for the field step of ±10 mT and were 98.99 ± 0.07 ms and 39.16 ± 0.04 ms for a field step of ±5 mT.

A third field sequence was performed on the FCS, centered at a field of 27 mT with a step of ±5 mT. Using this field range, both the maximum (32 mT) and minimum (22 mT) field are within the skyrmion stability pocket. At 32 mT the scattering pattern resolves to a hexagon imposed over a uniform ring, while at 22 mT the pattern is simply a hexagon. This could imply that the skyrmion lattice is dephasing and losing long-range orientation at the higher field. Alternatively, this could imply that the skyrmion lattice is dissolving to become skyrmions plus helices. Interestingly, the total integrated scattering intensity of these two states is conserved suggesting that the scattering is a result of the same structure and that dephasing is likely occurring; if helices were formed, the scattering form factor would change, resulting in a different intensity. Measurements performed on this sample previously [33] have similarly shown a ring plus hexagon scattering pattern at 40 mT which was resolved to a hexagon by rotating the sample in a static field, further supporting the conclusion that the ring originates from misoriented skyrmion domains. Time constants for dephasing of the skyrmion domains is reported to be 38 ms (stepping from 32 mT to 22 mT) while the reorientation to a single-domain configuration occurs in 58 ms (stepping from 22 mT to 32 mT).

Cu_2OSeO_3

The Cu_2OSeO_3 (COSO) sample has been shown to possess a magnetic skyrmion phase below the Curie temperature of 58 K.[35] Previous investigations on COSO have demonstrated its sensitivity to variations in external fields and temperatures, including the observation of multi-domain skyrmion lattices and the presence of two distinct skyrmion phases at different temperatures.[17, 36-38] In comparison to the other materials examined in this study, COSO exhibits the shortest time constants.

Measuring at 57 K, with the field applied along the [111] direction, a hexagonal scattering pattern appears at $q = (9.73 \pm 0.08) \times 10^{-3}$ Å^{-1} at a magnetic field of 17 mT (Fig. 3(a)) and then disappears at 33 mT,

corresponding to the lower and upper boundaries of the skyrmion stability envelope, respectively. Again the hexagonal pattern has azimuthal smearing, similar to the (Fe, Co)Si sample, indicating that the skyrmions form domains with limited rotational misorientation. Using a ±10 mT stepped field centered at 33 mT (the upper boundary), the scattering pattern evolved between a hexagon at 23 mT and no appreciable scattering at 43 mT. From the scattering intensity, the creation and destruction time constants were measured to be 26.8 ± 0.1 ms and 29.6 ± 0.1 ms, respectively. Investigating the lower boundary of the skyrmion stability envelope, the field was stepped between 7 mT and 27 mT, once again transitioning between a hexagon at 27 mT and no-appreciable scattering at 7 mT. From these data, the skyrmion lattice creation and annihilation time constants were measured as 37.1 ± 0.1 ms and 18.5 ± 0.1 ms, respectively.

The time constants for all of the creation and annihilation measurements are summarized in Table 1.

Discussion

This study investigates the ordering timescales for three different B20 skyrmion bulk materials: MnSi, FCS, and COSO. The SANS results show that the skyrmions form ordered hexagonal lattices over a surprisingly long timeframe (10's of miliseconds) and that these timeframes vary significantly between the three samples, with the fastest single events being 10.4 ms (MnSi, skyrmion lattice destruction at the upper field boundary, 38 mT step), and the slowest being 99 ms (FCS skyrmion lattice formation at the lower boundary, 5 mT field step). The formation and destruction timeframes from all of the measurements are tabulated in Table 1 and are consistent with the temperature-based measurements by Nakajima et al.[19] This relatively slow ordering may be the result of long-range coordination of skymion lattice domains. Specifically, the nucleation of skyrmion lattices is expected to occur spontaneously across the sample, with an orientation which is set by the magnetocrystalline anisotropy. As these domains grow and meet, they would likely be misaligned in their phase, and potentially also orientation, depending on the strength of the magnetocrystalline coupling. As the domains resolve their differences, these long-range magnetic motions may take a long time, resulting in dynamics which are much slower than conventional magnetic behavior. To capture this behavior with simulation and modeling presents a significant challenge in both simulation time and volume. Simulation was performed using the object oriented micromagnetic simulation (OOMMF) platform modeling a 3 nm thick film with lateral dimensions of 100×100 nm^2, 250×250 nm^2, 700×700 nm^2, using 1×1×1 cm^3 cells; these parameters were chosen to allow the simulations to be completed in a reasonable timeframe. Figure 4(a) shows the magnetic fluctuations (dm/dt) versus simulation time; the real space images and Fourier transforms for four select times in the 250 nm × 250 nm simulations are shown in panels (b-e). Indeed, with the increasing simulation size the simulation time (that is, the time that passes in the simulation space) required for convergence increases. Also, the 700×700 nm^2 shows several peaks on top of the longer decay which can be attributed to the nucleation and annihilation of the skyrmions and reorientation of the local ordering. While these models give an ordering time that is still much faster than our experimental results, it is consistent with our argument that larger sample volumes take longer to order. With this being the case, the ordering time becomes dependent on the magnetic energies, as well as the sample structure – and the ease with which the skyrmions can move in the material. While there is no absolute trend in the formation and destruction timeframes, COSO tends to be the fastest, while FCS is the slowest, and MnSi is in-between, following the average when taking a common field step of ≈10 mT.

The formation and destruction mechanics of the skyrmion lattice can be investigated in detail by evaluating the time-resolved structure of the diffraction peaks. Specifically, the peaks in the SANS pattern encode the average structure of the skyrmion lattice, with the peak location, e.g. radius in q, related to the inter-skyrmion spacing by the relationship $d = \frac{2\pi}{q}$ and the azimuthal angle corresponding to the long-range orientation of the hexagonal lattice. Naturally, variations in the lattice spacing will appear as

directional broadening of the peak in the radial direction, with larger real-space structure corresponding to smaller q, while variations in the lattice orientation appear as a broadening in the azimuthal direction. These trends are tabulated for an example case of MnSi at 28.8 K and a field step of 287.5 mT to 212.5 mT, corresponding lattice formation at the high-field boundary of the stability pocket and a field step of ±38 mT. The peak location, Fig. 5a, shows a slight increase with ordering time, indicating that the skyrmion lattice initially forms with a larger spacing than the static configuration. Translating these values to real-space lattice parameters, the inter-skyrmion spacing when first observed is 173 Å and quickly relaxes to its final value of 165 Å, a change of <5%. This behavior is consistent with established understanding that the skyrmion lattice period is determined by the ratio D/J, which does not change as the lattice is formed. Notably, during the domain growth process, the stray dipolar fields would be reduced, which in-turn reduces the equilibrium skyrmion size, consistent with the observed results. It is also interesting to note that the peak width for MnSi along the radial direction (Δq) has a more significant change, Fig. 5b, decreasing by ≈70% during the formation process. The peak broadening was approximately symmetric, implying that domains of skyrmions initially nucleate with much larger and smaller lattice parameters. This could indicate that skyrmions with a diameter of ≈165 Å form but suffer from a diminished packing factor, or more likely, that skyrmions which are particularly large or small nucleate to form local domains that relax over time.

Finally, the azimuthal distribution, $\Delta\phi$, Fig. 5c, also shows a decreasing trend, with the peak width decreasing by ≈50%, from 25° to 12°, during the formation. A width of 25° is notably large since the spacing between diffraction peaks is nominally 60°. This last trend suggests that the system initially nucleates several domains of ordered skyrmions with poor relative alignment, and as the ordering propagates, the relative orientation improves considerably. Since the magnetic field is applied along the skyrmion tubes, the in-plane orientation of the skyrmion lattice is determined by coupling to the underlying crystal lattice through the magnetocrystalline anisotropy. In these materials, the magnetocrystalline anisotropy is notably weak resulting in the poor initial ordering, but alignment improves as the domains grow and eventually intersect.

Similar trends are also observed for the other materials with FCS shown in Figs. 5d-f and COSO shown in Fig. 5g-i. The trend in the azimuthal width of the peaks, $\Delta\phi$, is much weaker in the FCS and COSO, and converge on much larger values, 40° and 50°, respectively, compared to ≈12° for MnSi. These much larger values indicate that the long-range orientation of the skyrmion lattice is much poorer in COSO and FCS. This may the result of a weaker magnetocrystalline coupling or increased magnetic pinning, particularly in the case of FCS. It may also indicate that the exchange interactions are generally weaker, allowing the magnetic structure to accommodate these effective domain boundaries. It is also notable that the data for the FCS do not extend to lower times since the fit would not converge for a six-peak model.

Discussing now the timescales of lattice formation and destruction, there are at-least four energy terms (exchange, DMI, magnetostatic, and magnetocrystalline), two independent variables (magnetic field and temperature) and two structural variables (chemical disorder, and defect density) which contribute to the ordering kinetics. Uniquely separating the contributions from each of these terms is beyond the scope of this work. To help elucidate the underlying physics, the timescales for the field steps are considered within each material. Using the 10 mT step as a fixed variable, comparisons are made between materials using the parameters tabulated in Table 2 for MnSi [39], COSO [40] and FCS [29].

For each material the data show that a larger field step results in a faster formation/destruction timeframe. For FCS the average formation and destruction timeframe was 71 ms and 28 ms for the 20 mT field step, and 86 ms and 49 ms for a 10 mT step, respectively. Also, for the MnSi, the average formation and destruction timeframe was 32 ms and 15 ms for a 75 mT step and 46 ms and 34 ms for a 25 mT step. This

can be easily understood by recognizing that the particular magnetic configuration is determined by the balance of the Zeeman (field) energy and the other energies within the system, including thermally induced fluctuations. Increasing or decreasing the field such that the system is far from its ground state configuration increases the energy difference between the instantaneous configuration and the thermodynamically stable arrangement. For a larger field step, small thermodynamically derived fluctuations will be sufficient to nucleate domains which will propagate faster as a result of the larger energy difference. This field dependence is observed both at the upper field boundary and lower field boundary of the skyrmion stability window. When comparing values within a material, most of the contributing energies are self-consistent. These energies may be influenced by conflating parameters, however, when comparing among the different materials.

Comparing among materials for approximately the same field step, it appears that higher temperatures result in faster ordering. Specifically, the average ordering times (average of formation and destruction) were 28 ms, 40 ms and 49 ms for COSO (T=57 K, ΔH= 20 mT), MnSi (T=28 K, ΔH= 25 mT) and FCS (T=20 K, ΔH= 20 mT), respectively. This behavior emphasizes the critical role that thermal fluctuations play in the ordering dynamics.

Comparing the trend in the speed (fastest to slowest, 28 ms, 40 ms, and 49 ms, for COSO, MnSi, and FCS, respectively) with the material-specific parameters summarized in Table 2, two more correlations emerge: (1) the formation time increases with the saturation magnetization (1.03 A/m, 1.63 A/m and 9.08 A/m for COSO, MnSi and FSC, respectively) and (2) the magnetocrystalline anisotropy (-0.6 J/m^3, 17 J/m^3 and 180 J/m^3 for COSO, MnSi and FSC, respectively). The dependence on the saturation magnetization is surprising, since each of the magnetic energies are linearly related to the magnetization (or spin); increasing M_S raises all of the energies. For the magnetocrystalline energy, one can consider the energy necessary to propagate the skyrmion lattice necessitates rotating spins through a magnetic hard axis, thus larger anisotropy corresponds to larger propagation energies and slower propagation. As reported previously in multilayers with perpendicular anisotropy, reducing the anisotropy increases the domain wall creep velocity.[41]

Finally, we consider the role of disorder in the system, which is chemical inhomogeneity in this case. While both MnSi and COSO are expected to be chemically homogeneous, the FCS sample has inherent disorder on the A-site, having a weighted random occupation of Fe and Co. Furthermore, the defect density of COSO is generally expected to be smaller than MnSi or FCS due simply to the former being a ceramic and the latter being an intermetallic compound. Both the compositional distribution and defect density can pin the skyrmions, slowing the ordering mechanics.[42] Indeed, FCS has the slowest ordering time, followed by MnSi, then COSO.

At this point it is important to note that these four parameters (saturation magnetization, magnetocrystalline anisotropy, disorder, and temperature) all show trends which are consistent with the observed formation and destruction times. However, from the provided data, it is not clear which of these are dominant in determining the timeframes, or even if any of them are; there may be no dominant parameter, but rather a combination, including correlations with the remaining variables in Table 2. These trendless-parameters may mix with the other parameters to determine the trend, or may simply be too small in the current systems. With this in mind, it is interesting to reflect on the parameters which do not show a clear trend in the formation and destruction in these data and why they should. First among these are the exchange and DMI terms, both of which are largest in MnSi, the medium speed material. Similar to the observed dependence on the magnetic field step, these terms increase the energy scale of the system such that being away from the ground state configuration presents a significant energy cost and should motivate rapid lattice formation and destruction. The ratio D/J determines the skyrmion size, which also

intuitively affects the ordering timeframes. Specifically, re-configuring large domains will take longer both due to their size, but also an inability to move freely among other skyrmions, e.g. a jamming. However, MnSi has the smallest skyrmions, despite being neither the fastest or slowest.

Another variable which might be expected to play a role in the ordering is the central field of the transition, relative to the upper or lower field transition. For the MnSi, the average ordering time at the upper field boundary is faster, while in FSC the lower field boundary is faster, and for COSO the ordering times are approximately the same. Knowing that the field step plays an important and clear role, larger fields corresponding to faster ordering, the upper field boundary might be expected to be faster. Alternatively, the upper field boundary is changing between the skyrmion state and a highly distorted conical structure, while the lower field boundary is transitioning to a much more relaxed conical – or even helical – state; resolving to different configurations might be expected to take different times.

In a final consideration, these measurements were performed on bulk-materials, which are treated as homogeneous, linear skyrmion tubes[43] in the preceding discussions. However, recent works[44, 45] have highlighted that the buried structure can be quite complex, including entanglement of tubes, non-topological skyrmion-like structures that terminate at either end, and branching between skyrmion tubes. Disentangling the tube may contribute significantly to the ordering timeframes. Previously, with these very samples, we have shown that rotating the samples can disentangle the skyrmions resulting in improved ordering.[33] This indicates that resolving these non-ground state configurations requires either additional external perturbation or much longer timeframes.[1] The density of these structures may be different if the system is adiabatically brought into and out-of the skyrmion stability window, versus the abrupt changes in these experiments. This would be consistent with the difference between our initial determination of the fields (which resulted in clean hexagonal scattering patterns) and the rings observed in the TRSANS results. The complement to these arguments is that it is also possible that some of these states do not have the time to dissolve in our field steps out of the skyrmion stability envelope. These residual structures would act as defects during the formation of the subsequent skyrmion lattice, introducing disorder and again causing spread in the scattering pattern.

Conclusion

In summary, we have used time-resolved small angle neutron scattering (TR-SANS) to investigate the ordering dynamics in three prototypical skyrmion materials: MnSi (space group B20), $Fe_{0.85}Co_{0.15}Si$ (space group B20) and Cu_2OSeO_3 (space group $P2_13$). The scattering patterns show that the ordering of the skyrmion lattices evolve asymptotically towards a stable configuration over a surprisingly slow timeframe of 10 ms - 100 ms. The ordering kinetics were determined by comparing the time-resolved diffraction patterns, including the diffraction peak location (q), its width Δq and its width in the azimuthal direction $\Delta\phi$. These results support a nucleation and growth model for the skyrmion lattices. The time-dependence of the ordering was also reported, with ordering occurring faster with larger field steps and increased temperature. These observations may indicate the role of thermal fluctuations within the system to accelerate the switching. Also, when increasing the saturation magnetization and magnetocrystalline anisotropy the ordering speed was reduced. These results confirm previous observations, that magnetic ordering in skyrmion lattices can be much slower than typical magnetic processes such as magnetic dynamics or domain wall motion and highlights trends in the material and measurement parameters which are consistent with the observed behavior.

ACKNOWLEDGEMENT

We appreciate discussions with Prof. Cristian D. Batista at the University of Tennessee, samples from Prof. Fang-Cheng Chou at National Taiwan University and SANS support from Cedric Gagnon at NIST. Neutron measurements and analysis were supported by US Department of Energy, Office of Science, Award DE-SC0021344. L.J.Q. was supported by the Center for High Resolution Neutron Scattering, a partnership between the National Institute of Standards and Technology and the National Science Foundation under Agreement No. DMR-2010792. A portion of this research used resources at the High Flux Isotope Reactor, a DOE Office of Science User Facility operated by the Oak Ridge National Laboratory.

AUTHOR CONTRIBUTION

Project and experiment design was performed by D.A.G., J.A.B. and L.D.-S. Samples were prepared by G.-J.H., F.-C.C. and N.P.B. SANS experiments were performed by W.L.N.C., N.T., L.Q, L.D.-S., M.B., J.A.B., K.L.K., A.J.G., and D.A.G. Simulations were performed by C.C.B. and D.A.G. Analysis of the results was performed by W.L.N.C., D.A.G., J.A.B., L.D.-S., and C.D.B. The first draft was written by W.L.N.C., and D.A.G. All authors made contributions to and approved the final text.

REFERENCES

[1] M. N. Wilson *et al.*, "Measuring the formation energy barrier of skyrmions in zinc-substituted Cu2OSeO3," *Physical Review B,* vol. 99, no. 17, p. 174421, 05/22/ 2019, doi: 10.1103/PhysRevB.99.174421.

[2] J. D. Reim *et al.*, "Impact of minute-time-scale kinetics on the stabilization of the skyrmion-lattice in Cu2OSeO3," *Journal of Physics: Conference Series,* vol. 828, p. 012004, 2017/04/20 2017, doi: 10.1088/1742-6596/828/1/012004.

[3] N. Tang *et al.*, "Skyrmion-Excited Spin-Wave Fractal Networks," *Advanced Materials,* vol. 35, no. 33, p. 2300416, 2023/08/01 2023, doi: https://doi.org/10.1002/adma.202300416.

[4] S. Seki *et al.*, "Formation and rotation of skyrmion crystal in the chiral-lattice insulator Cu2OSeO3," *Physical Review B,* vol. 85, no. 22, p. 220406, 06/22/ 2012, doi: 10.1103/PhysRevB.85.220406.

[5] A. Neubauer *et al.*, "Topological Hall Effect in the A Phase of MnSi," *Physical Review Letters,* vol. 102, no. 18, p. 186602, 05/04/ 2009, doi: 10.1103/PhysRevLett.102.186602.

[6] A. Fert, V. Cros, and J. Sampaio, "Skyrmions on the track," *Nature Nanotechnology,* vol. 8, no. 3, pp. 152-156, 2013/03/01 2013, doi: 10.1038/nnano.2013.29.

[7] W. Koshibae and N. Nagaosa, "Dynamics of skyrmion in disordered chiral magnet of thin film form," *Sci Rep,* vol. 9, no. 1, p. 5111, Mar 25 2019, doi: 10.1038/s41598-019-41441-5.

[8] Y. Hu, X. Chi, X. Li, Y. Liu, and A. Du, "Creation and Annihilation of Skyrmions in the Frustrated Magnets with Competing Exchange Interactions," *Scientific Reports,* vol. 7, no. 1, p. 16079, 2017/11/22 2017, doi: 10.1038/s41598-017-16348-8.

[9] D. A. Gilbert *et al.*, "Realization of ground-state artificial skyrmion lattices at room temperature," *Nature Communications,* vol. 6, no. 1, p. 8462, 2015/10/08 2015, doi: 10.1038/ncomms9462.

[10] S. Mühlbauer *et al.*, "Skyrmion Lattice in a Chiral Magnet," *Science,* vol. 323, no. 5916, p. 915, 2009, doi: 10.1126/science.1166767.

[11] S. X. Huang *et al.*, "Unusual magnetoresistance in cubic B20 Fe0.85Co0.15Si chiral magnets," *New Journal of Physics,* vol. 18, no. 6, p. 065010, 2016/06/24 2016, doi: 10.1088/1367-2630/18/6/065010.
[12] J. Müller, A. Rosch, and M. Garst, "Edge instabilities and skyrmion creation in magnetic layers," *New Journal of Physics,* vol. 18, no. 6, 2016, doi: 10.1088/1367-2630/18/6/065006.
[13] X. Yu *et al.*, "Aggregation and collapse dynamics of skyrmions in a non-equilibrium state," *Nature Physics,* vol. 14, no. 8, pp. 832-836, 2018, doi: 10.1038/s41567-018-0155-3.
[14] R. D. Desautels *et al.*, "Realization of ordered magnetic skyrmions in thin films at ambient conditions," *Physical Review Materials,* vol. 3, no. 10, 2019, doi: 10.1103/PhysRevMaterials.3.104406.
[15] A. Tonomura *et al.*, "Real-Space Observation of Skyrmion Lattice in Helimagnet MnSi Thin Samples," *Nano Letters,* vol. 12, no. 3, pp. 1673-1677, 2012/03/14 2012, doi: 10.1021/nl300073m.
[16] X. Yu *et al.*, "Magnetic stripes and skyrmions with helicity reversals," *Proceedings of the National Academy of Sciences,* vol. 109, no. 23, pp. 8856-8860, 2012/06/05 2012, doi: 10.1073/pnas.1118496109.
[17] L. J. Bannenberg *et al.*, "Reorientations, relaxations, metastabilities, and multidomains of skyrmion lattices," *Physical Review B,* vol. 96, no. 18, p. 184416, 11/13/ 2017, doi: 10.1103/PhysRevB.96.184416.
[18] M. Soda *et al.*, "Asymmetric slow dynamics of the skyrmion lattice in MnSi," *Nature Physics,* vol. 19, no. 10, pp. 1476-1481, 2023/10/01 2023, doi: 10.1038/s41567-023-02120-5.
[19] T. Nakajima *et al.*, "Phase-transition kinetics of magnetic skyrmions investigated by stroboscopic small-angle neutron scattering," *Physical Review B,* vol. 98, no. 1, p. 014424, 07/23/ 2018, doi: 10.1103/PhysRevB.98.014424.
[20] Charles *et al.*, "Sub-Millisecond Time-Resolved Small-Angle Neutron Scattering Measurements at NIST," (in en), *Journal of Applied Crystallography* 2020-06-03 2020. [Online]. Available: https://tsapps.nist.gov/publication/get_pdf.cfm?pub_id=929394.
[21] D. Mettus, A. Chacon, A. Bauer, S. Mühlbauer, and C. Pfleiderer, "Optimization strategies and artifacts of time-involved small-angle neutron scattering experiments," *Journal of Applied Crystallography,* vol. 55, no. 6, 2022.
[22] T. Y. Ou-Yang, G. J. Shu, C. D. Hu, and F. C. Chou, "Dynamic susceptibility study on the skyrmion phase stability of Fe0.7Co0.3Si," *Journal of Applied Physics,* vol. 117, no. 12, p. 123903, 2015/03/28 2015, doi: 10.1063/1.4915934.
[23] J. Barker *et al.*, "The very small angle neutron scattering instrument at the National Institute of Standards and Technology," *Journal of Applied Crystallography,* vol. 55, no. 2, pp. 271-283, 2022.
[24] S. Kline, "Reduction and analysis of SANS and USANS data using IGOR Pro," *Journal of Applied Crystallography,* vol. 39, no. 6, pp. 895-900, 2006, doi: doi:10.1107/S0021889806035059.
[25] C. Dewhurst, "Graphical reduction and analysis small-angle neutron scattering program: GRASP," *Journal of Applied Crystallography %@ 1600-5767,* vol. 56, no. 5, pp. 1595-1609, 2023, doi: doi:10.1107/S1600576723007379 %U https://doi.org/10.1107/S1600576723007379.
[26] A. Singh *et al.*, "Discretized evolution of solitons in the achiral stripe phase of a Fe/Gd thin film," *Physical Review B,* vol. 105, no. 9, p. 094423, 03/17/ 2022, doi: 10.1103/PhysRevB.105.094423.
[27] A. O. Leonov, "Precursor skyrmion states near the ordering temperatures of chiral magnets," *Physical Chemistry Chemical Physics,* 10.1039/D3CP03034B vol. 25, no. 42, pp. 28691-28702, 2023, doi: 10.1039/D3CP03034B.
[28] K. Ishimoto, Y. Yamaguchi, J. Suzuki, M. Arai, M. Furusaka, and Y. Endoh, "Small-angle neutron diffraction from the helical magnet Fe0.8Co0.2Si," *Physica B: Condensed Matter,* vol. 213-214, pp. 381-383, 1995/08/01/ 1995, doi: https://doi.org/10.1016/0921-4526(95)00163-4.

[29] S. V. Grigoriev, S. V. Maleyev, V. A. Dyadkin, D. Menzel, J. Schoenes, and H. Eckerlebe, "Principal interactions in the magnetic system Fe1-xCoxSi: Magnetic structure and critical temperature by neutron diffraction and SQUID measurements," *Physical Review B,* vol. 76, no. 9, p. 092407, 09/27/ 2007, doi: 10.1103/PhysRevB.76.092407.

[30] W. Münzer *et al.*, "Skyrmion lattice in the doped semiconductor Fe1-xCoxSi," *Physical Review B,* vol. 81, no. 4, p. 041203, 01/20/ 2010, doi: 10.1103/PhysRevB.81.041203.

[31] P. Bak and M. H. Jensen, "Theory of helical magnetic structures and phase transitions in MnSi and FeGe," *Journal of Physics C: Solid State Physics,* vol. 13, no. 31, pp. L881-L885, 1980/11/10 1980, doi: 10.1088/0022-3719/13/31/002.

[32] O. Nakanishi, A. Yanase, A. Hasegawa, and M. Kataoka, "The origin of the helical spin density wave in MnSi," *Solid State Communications,* vol. 35, no. 12, pp. 995-998, 1980/09/01/ 1980, doi: https://doi.org/10.1016/0038-1098(80)91004-2.

[33] D. A. Gilbert *et al.*, "Precipitating ordered skyrmion lattices from helical spaghetti and granular powders," *Physical Review Materials,* vol. 3, no. 1, p. 014408, 01/15/ 2019, doi: 10.1103/PhysRevMaterials.3.014408.

[34] J. E. Davies, O. Hellwig, E. E. Fullerton, G. Denbeaux, J. B. Kortright, and K. Liu, "Magnetization reversal of Co/Pt multilayers: Microscopic origin of high-field magnetic irreversibility," *Physical Review B,* vol. 70, no. 22, p. 224434, 12/29/ 2004, doi: 10.1103/PhysRevB.70.224434.

[35] N. Ogawa, S. Seki, and Y. Tokura, "Ultrafast optical excitation of magnetic skyrmions," *Scientific Reports,* vol. 5, no. 1, p. 9552, 2015/04/24 2015, doi: 10.1038/srep09552.

[36] A. Chacon *et al.*, "Observation of two independent skyrmion phases in a chiral magnetic material," *Nature Physics,* vol. 14, no. 9, pp. 936-941, 2018/09/01 2018, doi: 10.1038/s41567-018-0184-y.

[37] M. C. Langner *et al.*, "Coupled Skyrmion Sublattices in Cu2OSeO3," *Physical Review Letters,* vol. 112, no. 16, p. 167202, 04/25/ 2014, doi: 10.1103/PhysRevLett.112.167202.

[38] K. Makino *et al.*, "Thermal stability and irreversibility of skyrmion-lattice phases in Cu2OSeO3," *Physical Review B,* vol. 95, no. 13, p. 134412, 04/10/ 2017, doi: 10.1103/PhysRevB.95.134412.

[39] E. A. Karhu *et al.*, "Chiral modulations and reorientation effects in MnSi thin films," *Physical Review B,* vol. 85, no. 9, p. 094429, 03/27/ 2012, doi: 10.1103/PhysRevB.85.094429.

[40] P. Che *et al.*, "Confined dipole and exchange spin waves in a bulk chiral magnet with Dzyaloshinskii-Moriya interaction," *Physical Review Research,* vol. 3, no. 3, p. 033104, 07/30/ 2021, doi: 10.1103/PhysRevResearch.3.033104.

[41] P. M. Shepley, A. W. Rushforth, M. Wang, G. Burnell, and T. A. Moore, "Modification of perpendicular magnetic anisotropy and domain wall velocity in Pt/Co/Pt by voltage-induced strain," *Scientific Reports,* vol. 5, no. 1, p. 7921, 2015/01/21 2015, doi: 10.1038/srep07921.

[42] H. C. Choi, S.-Z. Lin, and J.-X. Zhu, "Density functional theory study of skyrmion pinning by atomic defects in MnSi," *Physical Review B,* vol. 93, no. 11, p. 115112, 03/07/ 2016, doi: 10.1103/PhysRevB.93.115112.

[43] W. L. N. C. Liyanage *et al.*, "Three-dimensional structure of hybrid magnetic skyrmions determined by neutron scattering," *Physical Review B,* vol. 107, no. 18, p. 184412, 05/05/ 2023, doi: 10.1103/PhysRevB.107.184412.

[44] M. E. Henderson *et al.*, "Three-dimensional neutron far-field tomography of a bulk skyrmion lattice," *Nature Physics,* vol. 19, no. 11, pp. 1617-1623, 2023/11/01 2023, doi: 10.1038/s41567-023-02175-4.

[45] P. Milde *et al.*, "Unwinding of a Skyrmion Lattice by Magnetic Monopoles," *Science,* vol. 340, no. 6136, pp. 1076-1080, 2013/05/31 2013, doi: 10.1126/science.1234657.

[46] G. Butenko, "Phenomenological theory of chiral states in magnets with Dzyaloshinskii-Moriya interactions," Dr.rer.nat., Dresden University of Technology, Dresden, 2013.
[47] D. Schroeter *et al.*, "MnSi nanostructures obtained from epitaxially grown thin films: magnetotransport and Hall effect," *Journal of Physics: Condensed Matter,* vol. 30, no. 23, p. 235805, 2018.
[48] B. Balasubramanian *et al.*, "Chiral Magnetism and High-Temperature Skyrmions in B20-Ordered Co-Si," *Physical Review Letters,* vol. 124, no. 5, p. 057201, 02/06/ 2020, doi: 10.1103/PhysRevLett.124.057201.
[49] S. Huang *et al.*, "Unusual magnetoresistance in cubic B20 Fe0. 85Co0. 15Si chiral magnets," *New journal of physics,* vol. 18, no. 6, p. 065010, 2016.
[50] I. Stasinopoulos *et al.*, "Low spin wave damping in the insulating chiral magnet Cu2OSeO3," *Applied Physics Letters,* vol. 111, no. 3, 2017.

Table 1

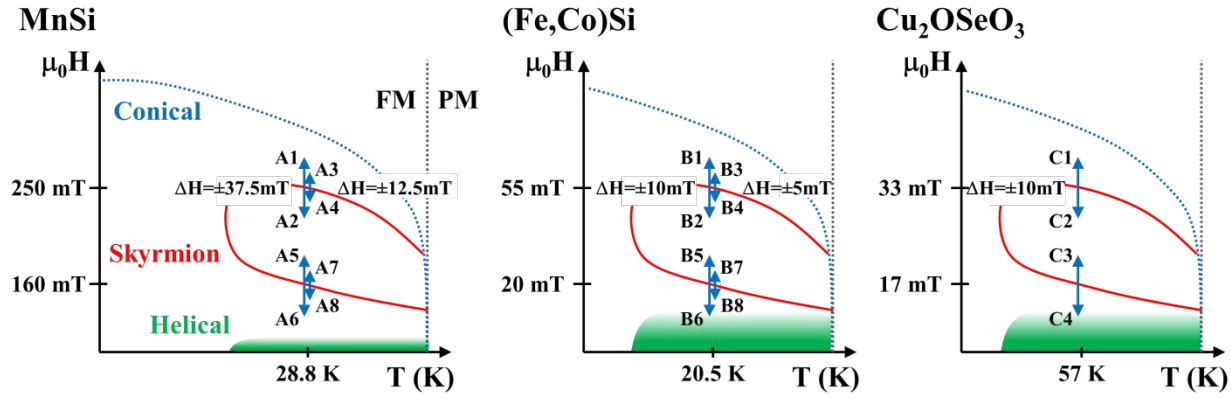

Sample	T (K)	State change		H (mT)	τ (ms)	Δτ (ms)
MnSi	28.8	A1: skx → con	Destruction	212.5 → 287.5	10.36	0.03
		A2: con →skx	Formation	287.5 → 212.5	42.71	0.04
		A3: skx → conical	Destruction	237.5 → 262.5	18.01	0.05
		A4: con →skx	Formation	262.5 → 237.5	47.78	0.04
		A5: con → skx	Formation	122.5 → 197.5	21.4	0.1
		A6: skx → con	Destruction	197.5 →122.5	18.97	0.02
		A7: con → skx *	Formation	147.5 →175.5	44.32	0.05
		A8: skx → con *	Destruction	175.5 →147.5	50.9	0.025
FCS	20.5	B1: skx → con	Destruction	45 → 65	35.49	0.03
		B2: con → skx	Formation	65 → 45	70.28	0.06
		B3: skx → con	Destruction	50 → 60	58.29	0.05
		B4: con → skx	Formation	60 → 50	72.1	0.06
		B5: heli → skx	Formation	10 → 30	71.19	0.05
		B6: skx → heli	Destruction	30 → 10	20.22	0.03
		B7: heli → skx	Formation	15 → 25	98.99	0.07
		B8: skx → heli	Destruction	25 → 15	39.15	0.04
COSO	57	C1: skx → con	Destruction	23 → 43	29.55	0.09
		C2: con → skx	Formation	43 → 23	26.8	0.09
		C3: con → skx	Formation	7 → 27	37.12	0.1
		C4: skx → con	Destruction	27 → 7	18.48	0.09

Table 1: Summary of the formation and destruction time constants with uncertainties for three samples. Abbreviations are used for skyrmion (skx), conical (con) and helical (heli). Diagram is provided to illustratively show respective measurements. *Skyrmion lattice not fully destroyed

Table 2

Sample	**M_S ($\times 10^5$ A/m)**	**A ($\times 10^{-13}$ J/m)**	**DMI ($\times 10^{-5}$ J/m^2)**	**K_U ($\times 10^3$ J/m^3)**	**d (Å)**	**D/A (nm^{-1})**	**R (T=T_C) (μΩ cm)**
MnSi	1.63	8.44	21.6	17[46]	164	0.406	29[47]
$Fe_{0.85}Co_{0.15}Si$	9.08	6.01	7.97	180[48]	410	0.133	331[49]
Cu_2OSeO_3	1.03	7.00	7.4	-0.6[50]	645	0.106	Insul.

Table 2: Saturation magnetization (M_S), exchange stiffness (A), DMI constant, magnetocrystalline anisotropy (K_U) values, skyrmion lattice parameter (d), D/A ratio, and resistivity (R) at T_C for each of the sample. Values are determined from experiment when possible and from literature when not. Insul=insulator, $>6\times10^{12}$ μΩ cm. All values were either measured or taken from Refs. [42]-[46]

Fig 1

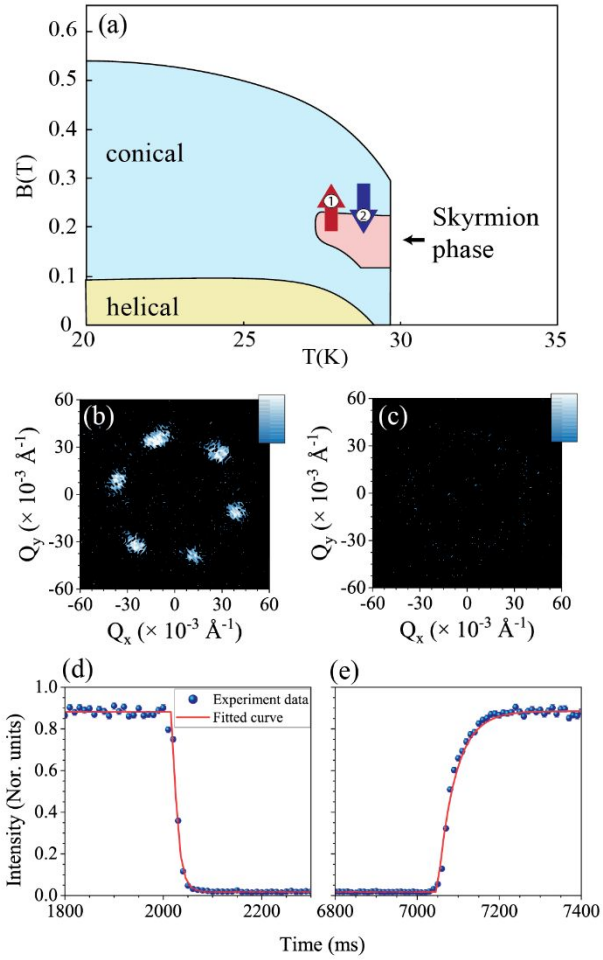

Figure 1: (a) The expected H-T phase diagram for MnSi [10] with the field step at the upper field boundary indicated by arrows labeled "1" for the increasing field (annihilation) and "2" for the decreasing (nucleation) events. The 2D small-angle neutron scattering (SANS) pattern measured (b) inside of and (c) outside of the skyrmion pocket during the dynamic field steps. The time-resolved integrated intensity showing (d) lattice destruction and (e) formation, with the fitted curves shown as a red line. Panels (b)-(e) were captured at 250 mT ±38 mT.

Fig 2

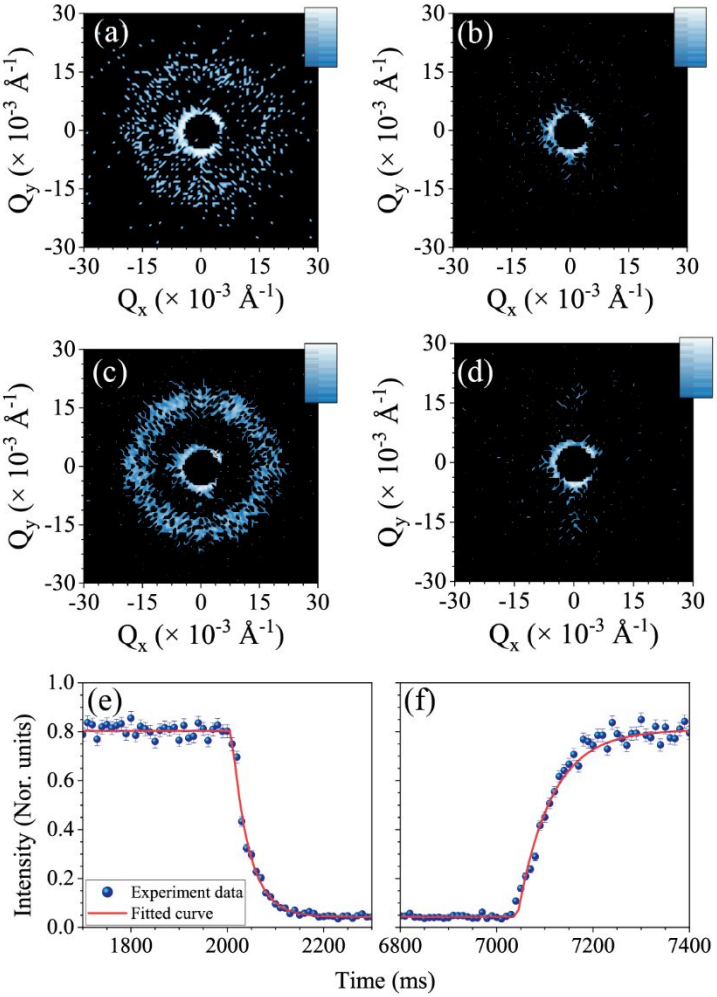

Figure 2: SANS data for FCS sample measured at the upper field boundary showing (a) ring type scattering pattern inside the skyrmion envelope and (b) suppressed scattering outside. Measurements at the lower boundary show (c) a hexagon imposed over a uniform ring inside the skyrmion stability window and (d) two weak diffraction peaks along the Q_y direction outside. The time-resolved integrated intensity showing (e) lattice destruction and (f) formation, with the fitted curves shown as a red line. Panels (a) and (b) were captured at 55 mT ±10 mT, while panels (c)-(f) were captured at 20 mT ±5 mT

Fig 3

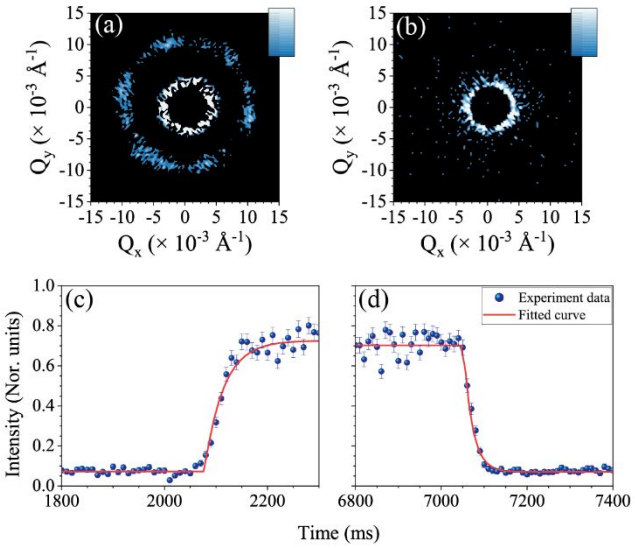

Figure 3: SANS pattern for COSO measured during the dynamic stepping, showing (a) a hexagonal scattering pattern representative of the skyrmion phase and (b) the diffuse scattering pattern measured outside the skyrmion stability window, in the conical phase. The time-resolved integrated intensity showing (c) lattice formation and (d) destruction, with the fitted curves shown as a red line. Panels (a)-(d) were captured at 55 mT ±10 mT

Fig 4

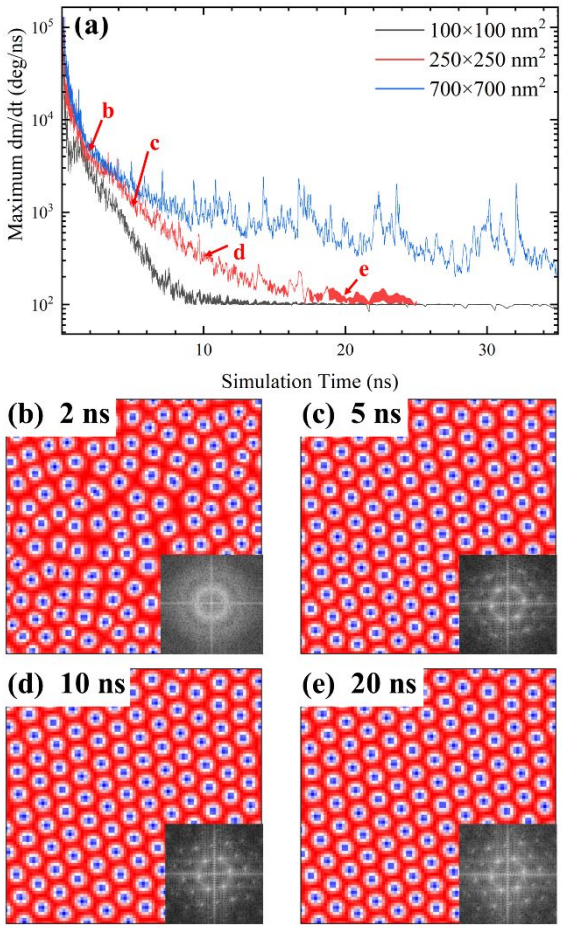

Figure 4: (a) Micromagnetic simulation results, showing magnetic fluctuations (dm/dt) as a function of simulation time. (b-e) Real space images and Fourier transforms (insets) of the magnetic configurations at 2 ns, 5 ns, 10 ns, 20 ns during the simulation.

Fig 5

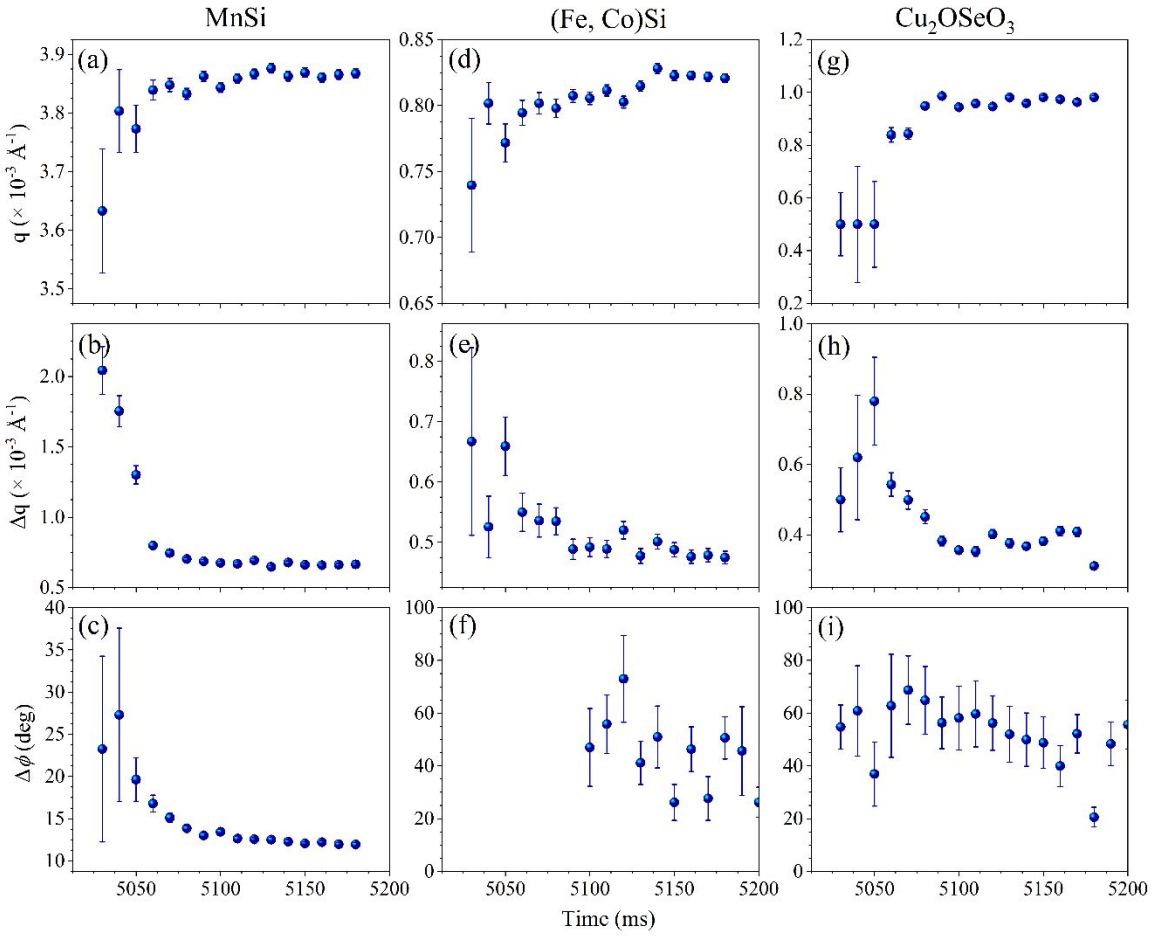

Figure 5: Example trends showing variation in the diffraction peaks in terms of their (top row) peak q-position, (middle row) peak width along the q-direction, Δq, and (bottom row) peak width, $\Delta\phi$, in the azimuthal direction. First column (a-c) is taken from MnSi at 28.8 K and a field step of 287.5 mT to 212.5 mT, second column (d-f) taken from FCO at 20.5 K and a field step of 65 mT to 45 mT, and (g-i) from COSO at 57 K and a field step of 43 mT to 23 mT. Error bars indicate the Standard Error, e.g. the Standard Deviation of the six peak widths divided by the square-root of six.